BACHELOR

The effect of the cathode radius on the neutron production in an IEC fusion device

Wijnen, M.

Award date:
2014

Bachelor Thesis

The effect of the cathode radius on the neutron production in an IEC fusion device

M.Wijnen
Eindhoven University of Technology

June 2014

Abstract

While magnetic confinement fusion is reaching the next level with the development of ITER, many other methods to achieve fusion are studied in parallel. One of these methods is inertial electrostatic confinement (IEC) which utilizes electrostatic fields to create fusion. The Eindhoven University of Technology operates the TU/e Fusor, modelled after a Hirsch-Farnsworth fusor. Two concentric spherical electrodes are placed in deuterium gas at near-vacuum, the inner electrode at a relative potential of -50 kV which allows for a plasma to form. As the inner electrode is near-transparent the ions engage in a radial oscillatory motion through the center of the device. During this oscillatory motion the ions may collide with the background gas allowing for either fusion or a loss reaction. The parameter to be investigated in this work is the cathode radius. Calculation shows that the beam-background fusion rate supposedly scales linearly with the cathode radius. The increase in cathode radius increases the distance where ions move at maximum velocity while concurrently decreasing the anode-cathode distance where they travel at sub-maximum velocities. Since loss mechanisms are predominant at lower energies this decreases loss reactions while increasing fusion reactions. The neutron production rate was found to scale with the voltage to the 3^{rd} to 4^{th} order. Doubling the grid radius favourably influences the NPR. A lack of theoretical models for the fusion rate impairs a more quantitative analysis.

Contents

1 Introduction

The concept of nuclear fusion was theoretically predicted in 1929 by R. Atkinson and F. Houtermans. Experimental verification followed shortly when in 1932 laboratory fusion of hydrogen isotopes was achieved for the first time [1]. Research on controlled nuclear fusion for civil purposes had to wait for almost two decades. Starting in the early 1950's more than seventy years of research eventually coalesced into ITER, an international project on what is soon to be the first thermonuclear fusion reactor yielding net power. ITER uses toroidal magnetic field to confine a plasma that sustains fusion, a concept that is known as a tokamak. Yet seventy years of research have produced more than one way to achieve fusion. Already in 1964, P.T. Farnsworth invented a device called the Farnsworth-Hirsch fusor (for later improvements made by R.L. Hirsch) which used inertial electrostatic confinement (IEC) to induce nuclear fusion. Although initial prospects where promising as the first fusors produced more fusion than any classical fusion device, funding was eventually reduced in favour of research on tokamaks. Although surprising at the time, it proved a choice for the better as later research showed that net power production is a practical impossibility for IEC devices. [2] In the early 1980s disappointingly slow progress on conventional nuclear fusion concepts sparked a renewed interest in alternative concepts including the fusor. While still unable to yield net power, it proved to be a viable neutron source. Recently the Eindhoven University of Technology (TU/e) built a fusor which serves a practical study object for students. The main objective of the TU/e Fusor is to explore the physics involved and maximize the neutron production. Up until now the fusor operated on merely 30% of the 120kV power supply, so there is obviously room for improvement. Also little is known about the influence of the size and shape of the cathode on the performance of the fusor. The aim of this bachelor thesis therefore is to investigate the effect of the cathode-radius on the neutron production.

2 Theory

2.1 Nuclear Fusion

The concept of nuclear fusion lies at the heart of all matter. It is the principle powering the sun and allows for nucleosynthesis. Positively charged nuclei repel each other. In order to fuse, the nuclei need sufficient energy to overcome the Coulomb-barrier. This means that at least one of the nuclei should be imparted with sufficient kinetic energy either by creating a high temperature as in thermonuclear fusion or by accelerating it in an electric field. When two light ($Z < 56$) nuclei fuse, they form a new element with a mass lower than the sum of the masses of the fusing nuclei. This mass deficit is released as energy following Einstein's famous equation $E = mc^2$. For $Z > 56$ there is a mass excess and it is more favourable for elements to split which is the concept of nuclear fission.

The nuclear fuel used in the TU/e Fusor is the hydrogen isotope deuterium. While some tritium is produced, deuterium-deuterium reactions dominate the process. D-D reactions have two possible outcomes. Both have a 50% chance to occur we, however are only interested in the second reaction which produces high energy (2.53 MeV) neutrons.

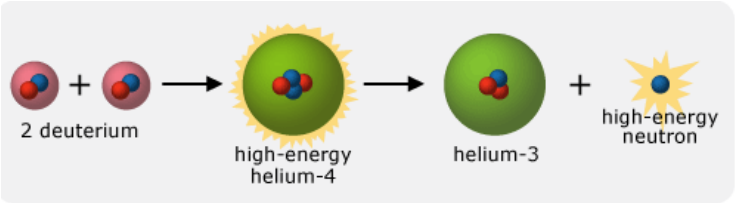

Figure 2.1: Neutron producing branch of the D-D fusion process

The height of the Coulomb-barrier is based on the inter-nucleic distance where the strong nuclear force takes over. The effective height of the barrier is affected by quantum tunnelling, incorporating this effect leads to an effective distance forming the radius of a circular surface, the fusion cross-section σ_f. The nuclei moving with a velocity v sweep a volume $\sigma_f v$ every second. If there is a velocity distribution usually a mean is calculated, the reactivity $\langle \sigma_f v \rangle$. Multiplying this by both particle densities yields the fusion probability.

$$P = n_1 n_2 \langle \sigma_f v \rangle \tag{2.1}$$

2.2 Hirsch-Farnsworth Fusors

The TU/e Fusor is a Hirsch-Farnsworth type IEC fusion device. These devices generally consist of two concentric spherically electrodes inside a vacuum vessel, although cylindrical and other configurations have been used. Inside the vessel a small fraction of ions reside either created by ionisation of a neutral gas or directly injected (the TU/e fusor employs the former method). The inner electrode is a near-transparent wire grid which functions as the cathode while the vessel itself is grounded and functions as the anode. By applying a negative potential to the cathode the positive ions are accelerated towards the grid and any electrons are accelerated towards the vessel wall. Because of the transparency of the grid most ions will overshoot the centre and reflect at the anode resulting in radial oscillatory motion of the ions.

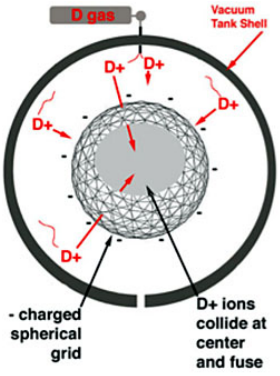

Figure 2.2: Schematic overview of a fusor

2.3 Vacuum Potential

When a voltage is applied to the cathode a potential difference between cathode and anode is created. The so-called vacuum potential profile $\Phi(r)$ is dependent on the distance to the cathode, denoted r. For two concentric spheres the vacuum potential is given by equation 2.2.

$$\Phi(r) = \frac{\Phi_c}{1 - \frac{R_a}{R_c}} \left[1 - \frac{R_a}{r}\right] \tag{2.2}$$

In the above equation R_c and R_a are the anode and cathode radius respectively and Φ_c is the cathode potential. Figure 2.3 shows a plot of this equation. The inner sphere in the fusor however, is a near-transparent grid. Simulation of this geometry yielded a slightly different potential profile as can be seen in figure 2.4.

The upper line in figure 2.4 is the potential on a trajectory through a grid opening, while the lower line is the potential on a trajectory through a grid wire. Comparison of the simulated and calculated potential profiles show two apparent differences. The potential profile is dependent on the angle and the constant potential inside the cathode is higher than the applied potential. Assuming that in star-mode the majority of the ion flow is on a line through a grid opening only the upper lines in figure 2.4 are of concern. The increased potential inside the cathode implies that the ions are accelerated over a smaller potential difference than the applied voltage and therefore have a lower maximum energy.

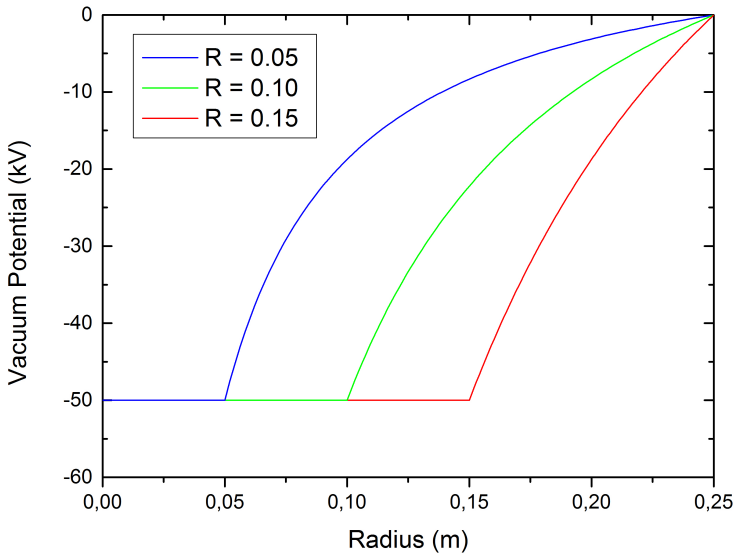

Figure 2.3: Calculated vacuum potential profile for different grid radii

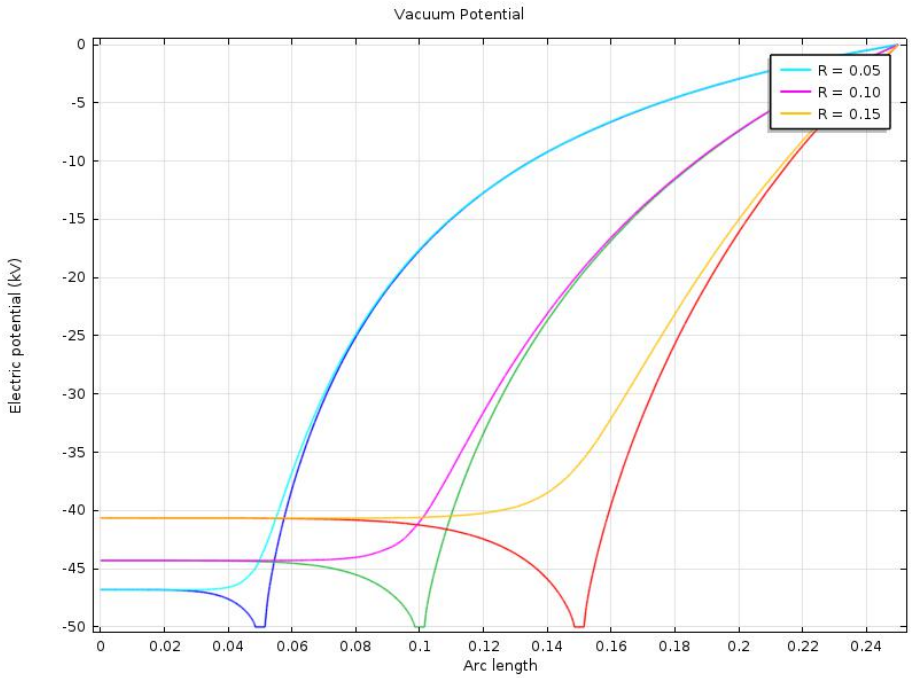

Figure 2.4: Vacuum potential profile simulations for different grid radii

2.4 Discharge

The ion source in the TU/e fusor is a plasma formed by the (partially) ionized background gas. At sufficient pressure and voltage, the applied electric field causes a gas discharge. A small amount of seed electrons around the cathode accelerat due to the field and ionize deuterium atoms. Every ionization frees up an electron thereby creating an ion. The created electron and ion then accelerate in opposing directions colliding with other atoms which again can lead to ionisation, respectively referred to as electron-impact (EII) and ion-impact ionisation (III). Ions colliding onto the cathode can also free up electrons which is referred to as secondary electron emission (SEE). The resulting ionisation cascade is called a Townsend avalanche. The occurrence of a gas discharge is dependent on the number of collisions, the energy gained by the electrons and the ionization probability. The parameters corresponding to these factors are the pressure, the electric field and the type of gas. The applied voltage at which a discharge occurs is called the breakdown voltage. In a parallel plate geometry the relationship between these parameters is given by the Paschen curve.

$$V_b = \frac{A(pd)}{\ln(Bpd) - \ln\left(\ln\left(\gamma^{-1} + 1\right)\right)} \tag{2.3}$$

A plot of the Paschen Curve for a electrode distance of 15 cm is shown in figure 2.5 where the coefficients A and B for Deuterium are 173 $V \cdot (Pa \cdot m)^{-1}$ and 7 $(Pa \cdot m)^{-1}$ respectively. The secondary Townsend coefficient, γ, of the nickel electrode has a value of 2.

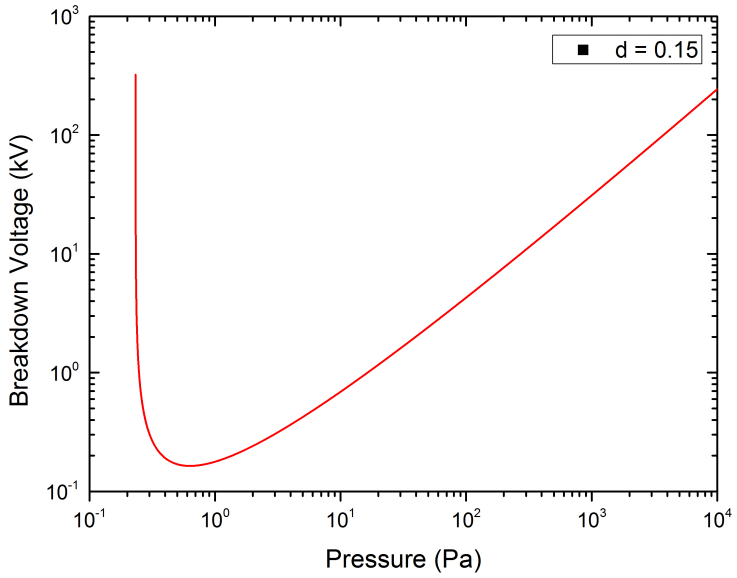

Figure 2.5: Paschen curve for deuterium

However for the spherical geometry of fusor this is not a valid relationship [3] as Paschen's Law is based on a homogenous electric field. Although measurements

of the breakdown voltage show similar behaviour an empirical scaling law has been derived which holds for a spherical geometry. [4]

$$V_b \approx \frac{0.21 \cdot A}{(pd)^2} \tag{2.4}$$

Here A is the atomic mass of the fuel species, p the pressure and d the distance between cathode and anode. Plotting V as a function of $A/(pd)^2$ should yield a straight line through the origin with a slope of 0.21 $kV \cdot Pa^2 \cdot m^2 \cdot amu^{-1}$.

2.5 Ion Current

As long as the discharge is maintained ionization takes place. For every ion created there is also an electron created which is absorbed at the wall. We define the cathode current I_c as the current corresponding to this process, as the same (ion)current is incident on the cathode surface. The cathode current however is not a parameter that can be monitored directly and therefore has to be linked to the total current I. The total current consists of the cathode current, thermionic emission, secondary electron emission, photoelectric and field-emission currents. The photoelectric current is due to bremsstrahlung incident on the vessel wall and field-emission is caused by electric fields at non-smooth surfaces. Both are difficult to account for, are assumed small and will therefore be left out of this discussion. [4] We are then left with:

$$I = I_c + I_{th} + I_\gamma \tag{2.5}$$

The thermionic emission is given by the Richardson-Duschman equation:

$$I_{th} = \Lambda_c A T^2 e^{-W/k_b T} \tag{2.6}$$

Where A is the surface area of the grid, T the temperature, k_B the Boltzmann constant and Λ_c the material specific Richardson coefficient, lastly W is the work function of the grid material. For nickel, the grid material of choice in the TU/e Fusor W and Λ_c are 5.01 eV [5] and $0.30 \cdot 10^6 Am^{-2}K^{-2}$ respectively. For a grid with a radius of 0.10 m consisting of nine 1 mm wires at 1000 K the thermionic emission current is around $3.1 \cdot 10^{-16} A$ which is negligible compared to the circuit current which is of the order of $10^{-3} - 10^{-1}$ A.

The secondary electron current is the current formed by the electrons which are freed up from the cathode by ions incident on the grid $I_\gamma = \gamma I_c$. Combining this with equation 2.5 leads to a definition of the ion current

$$I_i = \frac{I}{1+\gamma} \tag{2.7}$$

Ion Flux

The ion flux at the cathode ϕ_i is defined as the ion current divided by the elementary charge and the cathode surface. It represents the amount of ions per second penetrating the cathode volume.

$$\phi_i = \frac{I_i}{e v_c A} \tag{2.8}$$

2.6 Confinement

Confinement is an important parameter in nuclear fusion usually expressed as confinement time, the time particles are confined in the plasma. In IEC devices confinement is achieved by the inherent focal character of the spherical device. The recirculation is a measure for the confinement time in an IEC device. It prolongs their lifetime and is defined as the number of passes an ion makes before it is lost. For a given geometric transparency η only $\eta\phi_i$ enters the cathode volume, $\eta^2\phi_i$ passes through and $\eta^3\phi_i$ re-enters the cathode again on the second pass. This results in a converging geometric series which will be referred to as the *recirculation* Γ.

$$\Gamma = \eta + \eta^3 + ... = \sum_{n=0}^{\infty} \eta^{2n+1} = \frac{\eta}{1-\eta^2} \tag{2.9}$$

However this does not account for other loss reactions which may reduce the number of passes.

2.7 Collision Processes

Due to the recirculation of ions in the fusor collisions are bound to occur. Ions can collide with other ions or with neutral atoms. There exists a plethora of reactions that are possible between different species of ions and atoms. All reactions have different cross sections dependent on the energy of the reactants as shown in figure 2.6.

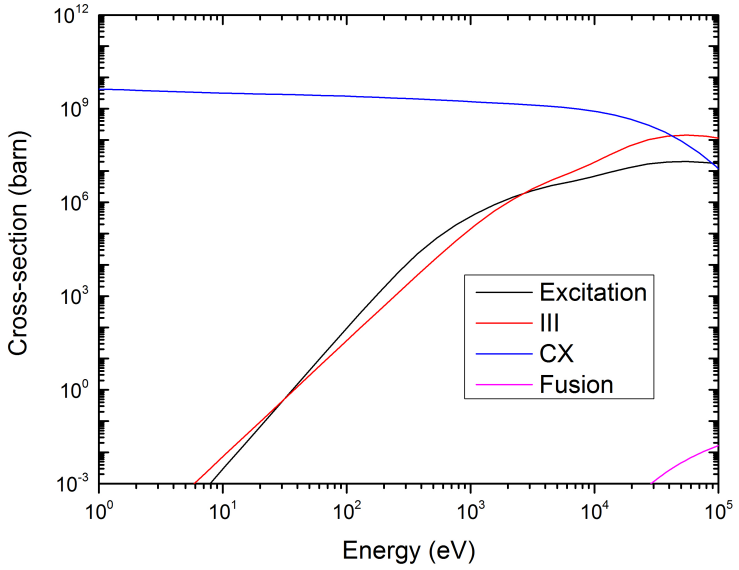

Figure 2.6: Cross-sections of the collisional processes

Ions colliding with a neutral atom can excite the atom to a higher state, where the ion loses energy to the atom which in turn is radiated as a photon. This

process is simply referred to as excitation. Another reaction between ions and neutral atoms is charge exchange whereby the atoms transfer an electron to the ion effectively creating a slow ion and a fast-neutral. The third reaction possible that can occur between neutrals and ions is ion-impact ionisation. The atom is ionised, freeing up one electron and creating a second ion, the incident ion however loses part of its energy. The aforementioned reactions are all loss reactions meaning that the high-energy incident ion loses part of its energy and is thereby excluded from causing further fusion reactions. The fourth reaction is the fusion reaction. In figure 2.6 the cross sections of all four reactions are plotted as a function of the ion energy for comparison of the reaction probabilities.
For the fusion reaction three types of reactants have to be considered, beam ions which are ions converging on the centre, fast neutrals which are created by charge exchange and background neutrals which are the atoms in the stationary background gas. Earlier research has shown that beam-background reactions are the dominant fusion reaction and all others can be neglected. [3]

2.8 Velocity Distribution

The cross section as a function of the velocity $\sigma(v)$ is a property of the D-D fusion reaction, the velocity distribution $f(v)$ however is not. In IEC devices in general and in Hirsch-Farsnworth fusors particularly there is no thermalisation and therefore no Maxwellian distribution. The velocity distribution is most likely very much dependent on the specific configuration and any general relationship has yet to be produced. However some assumptions can be made. The potential inside the cathode is constant and the velocity distribution (inside the cathode) is therefore assumed constant as well. Furthermore the maximum velocity, neglecting up-scattering is dependent on the applied potential.

$$v_{max} = \sqrt{\frac{2eV}{m}} \tag{2.10}$$

However it was already shown in figure 2.4 that the potential inside the cathode is not equal to the potential of the grid. For any calculations it is convenient to calculate a mean velocity or mean reactivity by multiplying by the velocity distribution and integrating over the domain.

$$\langle ... \rangle = \int_0^{v_{max}} ... f(v) dv \tag{2.11}$$

2.9 Fusion rate

The fusion rate is dependent on the amount of collisions and the fusion probability. The latter is given by equation 2.1 and scales with the number densities of both reactants as well as with the reactivity $\langle \sigma_f v \rangle$. For beam-background fusion the reactants are the beam ions and the background molecules. The number density of the background gas is given by the ideal gas law $p = nk_BT$, for a well cooled spherical vessel of $R = 0.25\ m$ at room temperature ($293\ K$) the density is a linear function of the pressure $n_{bg} = 2.42 \cdot 10^{20} \cdot p$. The number density

of the beam ions is dependent on the ion flux, the recirculation and the mean velocity at the cathode.

$$n_b = \langle \phi_i \rangle \, \Gamma = \frac{I}{1+\gamma} \frac{\Gamma}{4\pi R_c^2 e} \langle v \rangle_c^{-1} \tag{2.12}$$

From equation 2.12 it is clear that the beam number density scales linearly with the current as well as with the recirculation. Substituting both number densities in equation 2.1 and multiplying by the cathode volume yields the fusion rate F.

$$F = \frac{p}{k_B T} \frac{I}{(1+\gamma)e} 2R_c \Gamma \frac{\langle \sigma_f v \rangle_c}{\langle v \rangle_c} \tag{2.13}$$

$$F \approx 10^{39} \cdot pIR_c \Gamma \frac{\langle \sigma_f v \rangle_c}{\langle v \rangle_c} \tag{2.14}$$

Note that the volume is represented by a cylindrical projection with base $4\pi R_c^2$ and height $2R_c$. As mentioned in 2.1 only half of the fusion reactions produces a neutron. The neutron production rate (NPR) is a measurable quantity representative of the fusion rate related by $F = 2 \cdot NPR$.

2.10 Plasma Modes

In ealier work on the TU/e Fusor [3] it was established that the device had three distinct operating regimes depending on the pressure. At high pressures ($> 10\ Pa$) an azimuthaly uniform glow discharge exists both inside and outside the cathode, also called 'glow mode'. Between $1-10\ Pa$ the discharge is confined to the inside of the cathode accompanied by a plasma jet through one of the grid openings, aptly referred to as 'jet mode'. At low pressures ($> 1\ Pa$) the discharged exists only of spokes through opposing grid openings, which are called microchannels. The microchannels intersect in a bright core region in the center of the cathode. This last mode which is referred to as 'star mode' has the highest confinement and is deemed most suitable for neutron production.

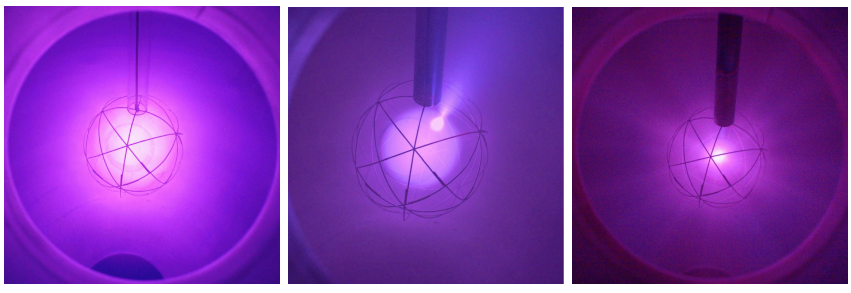

(a) Glow mode (b) Jet mode (c) Star mode

Figure 2.7: TU/e Fusor operating modes

Microchannels

Microchannels are the trajectories through two opposing grid openings where most of the discharge is confined in star mode operation. As of yet there are no conclusive theories about microchannel formation. One proposed theory is that microchannels form by self-selection. Ions born on a trajectory passing through or near the grids wires are quickly eliminated while those on a trajectory through or near a grid opening recirculate repeatedly leading to increased ionization along this trajectory. The department of Science and Technology of Nuclear Fusion at the TU/e is currently investigating whether micro-channel formation can be described by an electrostatic lens effect similar to an Einzel lens. Research has shown that microchannel formation greatly influences the transparency [6]. Recirculation therefore is dependent on a so-called effective transparency rather than the geometric transparency, however no quantitative relationship is known.

2.11 Grid Characteristics

The grid is the most fundamental part of IEC devices. The transparency as has been mentioned before is responsible for the recirculation of the ions which is the underlying mechanism of the device. Under certain conditions the grid also allows for microchannel formation which effectively increases the transparency to near unity. It also allows for the formation of a multiple potential well inside the cathode which is suspected to play an important roll in the efficiency of the device. The grid has certain characteristics, most important are the shape, size, wire configuration material and transparency. All have a distinct effect on the workings of the fusor and will be discussed separately.

Shape

Although all shapes are theoretically possible, most research has been done on cylindrical and spherical grids. Single ring grids have also been used as a simplification of both the spherical and cylindrical configurations. While both shapes have been shown to produce nuclear fusion, spherical shapes have a higher yield [7]. This is explained by the difference in convergence between sphere and cylinder. However cylindrical devices are easier to upscale as their length is easily increased.

Wire Configuration

Another important characteristic (for any shape) is the wire configuration. This determined by the amount of wires and the way the wires are connected. The most important effect of the wire configuration is the formation of micro-channels which is favoured by a configuration with opposing holes. However the configuration is often constrained by manufacturing ability. Two widely used configurations are the geodesic and the latitude-longitude configuration. Murali and colleagues have shown that there is no significant difference in neutron production for these configurations [6].

Geometric Transparency

The geometric transparency is affected by the number of wires and the wire thickness. It is defined as the surface of the sphere minus the surface of the wires divided by the surface of the sphere which translates to equation 2.15 where w is the wire thickness and N the number of wires.

$$\eta = 1 - \frac{Nw}{2R_c} \tag{2.15}$$

Although the geometric transparency was long be assumed a leading factor in the efficiency, research on micro-channels has shown that the resulting effective transparency exceeds the geometric transparency.

Material

As a cathode the grid has to be conductive and therefore the materials of choice are usually limited to metals. Favourable grid materials have a high melting temperature, low sputtering yield, a high work function, a low secondary electron emission (SEE) coefficient and have to be economic and practical. Sputtering contaminates the process and is to be avoided. The high work function and low SEE coefficient keep the thermionic emission current and SEE currents as low as possible. Grid temperatures often exceed $1000K$ so the grid material needs to have a sufficiently high melting point. The reactive metals rhenium, tantalum, tungsten and molybdenum have many of the desirable properties. However for economic and practical reasons often nickel or stainless steel is used.

Size

The grid size is the parameter to be investigated in this report. As shown in paragraph 2.6 loss reactions dominate at lower energies. As the fusion probability is a monotonous increasing function of the energy (in the range of the experiment) accelerating the ions to the maximum velocity as fast as possible increases the fusion probability. Increasing the grid radius changes the electric field and therefore the acceleration of the ions, which is given by equation 2.16

$$a = \frac{q}{m}\frac{dV}{dr} \tag{2.16}$$

Where q is the charge of the ion and m its mass, dV/dr is the electric field in the radial direction. From figure 2.4 it is evident that for an increasing grid radius, dV/dr increases. It is therefore expected that increasing the radius has a positive effect on the fusion probability. However fig 2.4 also shows that the potential in the center of the fusor is higher than the grid potential which translates to a lower maximum ion-velocity and therefore a lower fusion probability. The increase in cathode radius increases the distance where ions move at maximum velocity while concurrently decreasing the anode-cathode distance where they travel at sub-maximum velocities. Since loss mechanisms are predominant at lower energies this decreases loss reactions while increasing fusion reactions.

Based on 2.13 the hypothesis is that the fusion rate is a linear function of the grid radius. However too little is known about the physics of the fusor and the velocity distribution in particular to predict the exact effect of increasing the grid radius.

3 Experimental Setup

3.1 General Setup

The TU/e Fusor is a large set-up taking up a full room. This is mainly because of operation at high-voltage for which a grounded cage is mandatory. The general set-up is shown in figure 3.1 and consists of three subsystems: high-voltage system, the vacuum system and the diagnostics.

High-Voltage System

The HV-system consists of the power supply unit (PSU) in series with a 210 $k\Omega$ resistance stack to guarantee stability of the discharge and connected to the cathode by means of a HV feed-through. The vacuum chamber is grounded and serves as the anode. The PSU is a Heizinger HCN that can deliver up to 120 kV at 100 mA. The feed-through is validated up to 65 kV but in practice is able to handle up to 90 kV.

Vacuum System

The vacuum system consists of a 0.50 m diameter spherical vacuum chamber, which is emptied by a Pfeiffer HiCube 80 vacuum pump; a combination of a roughing pump and a turbo-molecular pump. Taking leaks into account a pressure of $2.2 \cdot 10^{-2}$ Pa can be attained. Also connected to the vacuum chamber is a gas-inlet, regulated by a needle valve. Although any type of gas can be connected in this work only deuterium is used.

Diagnostics

The denominator diagnostics entails a variety of devices, some specific to the research others mandatory for general fusor operation. In the last category are the pressure gauge, camera and radiometers. Connected in parallel to the gas-inlet is a Pfeiffer IMR 265 process ion gauge which operates a Pirani and a hot-cathode detector depending on the pressure range. This gauge is connected to a Pfeiffer TPG 262 measurement and control unit which processes the data from the gauge. This combination covers the pressure range from $2 \cdot 10^{-4} - 2 \cdot 10^{5}$ Pa. Connected to one of the view ports is a Logitech C525 HD webcam that allows for live imaging of the plasma. Two Thermo FH40G dose rate measuring units monitor the bremsstrahlung coming from the fusor. To monitor the neutron production a Studsvik 2202D dose rate meter is used which displays the dose

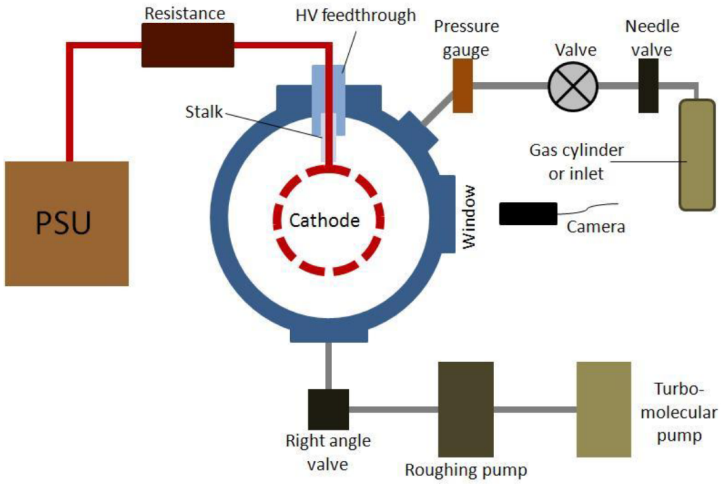

Figure 3.1: Schematic overview of the TU/e Fusor set-up

rate in $\mu Sv/h$ and also outputs a TTL pulsed signal that is routed to a counter. Voltage over and current through the set-up as a whole can be read of the PSU, the voltage over the fusor can be obtained computationally. The additional view ports allow for spectroscopy, Langmuir-probes and other diagnostics which will not be used in this research.

3.2 Grid Properties

The aim of this report is to investigate the effect of the grid radius on the neutron production rate. To this end three cathode grids of differing radii are produced from 1 mm nickel wire. The grids have a radius of 0.05, 0.10 and 0.15 m respectively. Initially every grid was designed to have the same geometric transparency using a combination of wires of different thickness. However this lead to overheating of thinner wires and a general absence of 'star-mode' in certain configurations. Since effective transparency caused by micro-channel formation outweighs the geometric transparency, the ability to produce 'star-mode' was given priority resulting in varying transparencies. All grids have the same 9-wire geodesic configuration for practical reasons. Wehmeyer et al. [8] have shown that there is no significant difference in neutron production rate between geodesic and latitude-longitude configurations. The transparencies and the associated 'recirculation' of the grids are given in the table below.

Grid Radius [m]	Transparency [%]	Recirculation
0.05	91	5.29
0.10	95.5	10.86
0.15	97	16.41

Table 3.1: Grid characteristics

3.3 Measurement Plan

For all grids three types of measurements are to be conducted. Firstly the breakdown characteristics are investigated to find the operating range of each grid and to verify Hochberg's scaling laws [4]. By ramping the voltage until a current is detected the breakdown voltage V_B is found for different pressures. Secondly the neutron production rate (NPR) will be measured as a function of the voltage at several different pressures. The lower boundary of the pressure range was chosen based upon the breakdown characteristics to be as low as possible but still allow for measurements over a sufficient range of voltages. At higher pressures current tends to soar and the voltage output of the PSU is current limited. Taking this in consideration for the upper bound, the resulting pressure range is $0.60 - 0.40\ Pa$ in $0.05\ Pa$ increments. Lastly the NPR is measured as a function of pressure at $80\ kV$. This is the highest possible voltage that allows operation without causing rated breakdown in the feed-through.

3.4 Automated Data Acquisition

To allow for accurate and fast data acquisition the measuring process was automated as much as possible. The PSU unit has a coaxial interface that relays information about the current and voltage and also allows for controlling the applied voltage. A duplicate of the IMR265 output voltage was relayed from the TPG 262. The neutron dose meter's coaxial output with a rudimentary TTL pulsed signal was used for measuring the NPR. All signals are connected to a NI PXIe-6361 DAQ unit which in turn was connected to a NI PXIe-8133 system. The web-cam is also connected to the PXIe-8133 by means of a USB-port. Two different executables were developed with LabView to control the experiments mentioned in section 3.3.

3.5 Data Processing Methods

All the acquired data are real-time plots of all parameters associated with the measurement. The acquired data was uploaded in Origin 9.0 and fitted to extract single values representative of that particular measurement. For determining the breakdown voltage, the voltage ramp was fitted with a linear fit to find a parametrization. Then the time value at which the current started to increase monotonously was found by inspection. Lastly the breakdown voltage was calculated by substituting the time-value in the parametrization. The accompanying pressure was found by fitting a straight line through pressure on the time-interval before breakdown. The pressure is assumed constant over the measurement period as outflow of gas is negligible on these time scales. During breakdown certain artefacts occur which make fitting over the total interval unrepresentative of the actual pressure. For both NPR measurements the voltage and current are fitted with a straight line on an interval where both parameters are constant. The neutron count is fitted on the same interval with a linear function; the slope represents the counts per second (cps). Figures 3.2 and 3.3 show a graphical representation of the fitting methods.

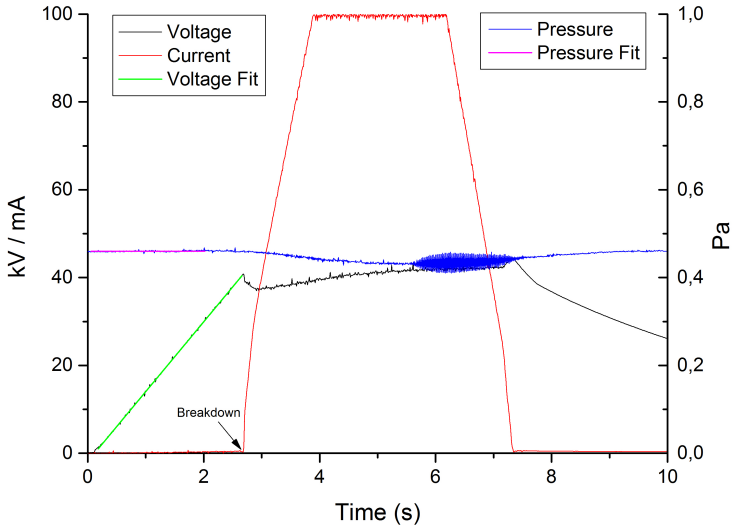

Figure 3.2: Breakdown measurement fitting graph

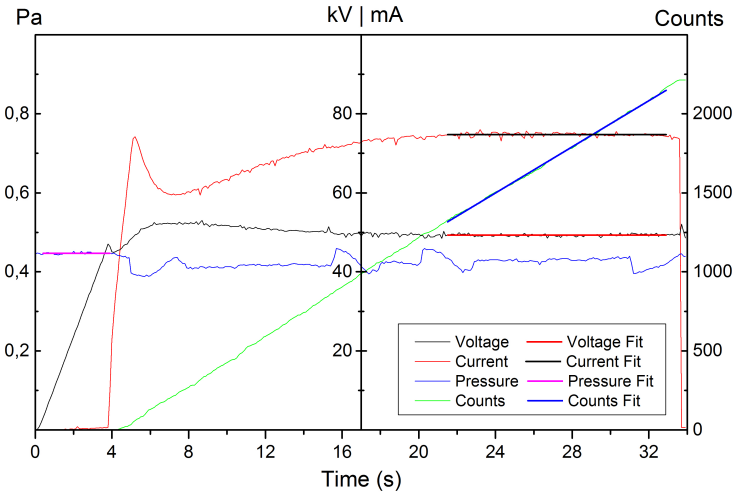

Figure 3.3: NPR measurement fitting graph

3.6 Error Estimates

Four main parameters, voltage, current, pressure and neutron count, are measured in the experiments which consequently have measuring errors. These errors can be divided in systematic and random errors. This section will discuss the source and estimate of the errors for all four parameters.

Voltage and Current

Both the current and voltage are internally measured by the PSU and converted to a $0 - 10V$ output. To asses the systematic error the voltage supplied by the PSU was measured directly with a HV-probe and compared to output of the software. A systemic error of $+0.2kV$ was found. Similar measurements could not be conducted for the current. As the plasma conditions are variable in time it is impossible to conduct a series of measurements on repeatability. Therefore a relative error of ± 1 kV and ± 1 mA on both the current and voltage, which is likely an overestimation.

Pressure

The repeatability of the IMR265 according to the manual is about 2%. Although probably an overestimation, it is chosen as the relative error on the pressure. No measurements have been conducted to establish a systematic error.

Neutron Production Rate

The neutron production rate is calculated from the pulse count of the neutron meter. The counts per second (cps) is defined as the slope of total count as a function of time which has an error Δcps. To calculate NPR the cps is divided by the sensitivity of the Studsvik dose rate meter which has a value of $0.5 \pm 0.01 cps$ per neutron$/s \cdot cm^2$ and multiplied by the area of the sphere with the distance between the center of the fusor and the neutron detector as its radius. The complete error calculation for the NPR is given by equation 3.1 below.

$$\left|\frac{\Delta NPR}{NPR}\right| = \left|\frac{\Delta sens}{sens}\right| + 2\left|\frac{\Delta r}{r}\right| + \left|\frac{\Delta cps}{cps}\right| \tag{3.1}$$

The distance of the center of the fusor to the center of the detector was measured 42 ± 1 cm the sensitivity of the detector according to the manual is $50 \pm 5 \cdot 10^{-2} cps$ per nps/cm^2.

4 Breakdown Characteristics

4.1 Results

To define the operating range for the NPR experiments the breakdown characteristics were investigated using the set-up described in chapter 3. Figure 4.1 shows a plot of the breakdown voltage as a function of the pressure for the 0.10 m and 0.05 m grids. The parallel plate Paschen curves for both electrode distances are also plotted.

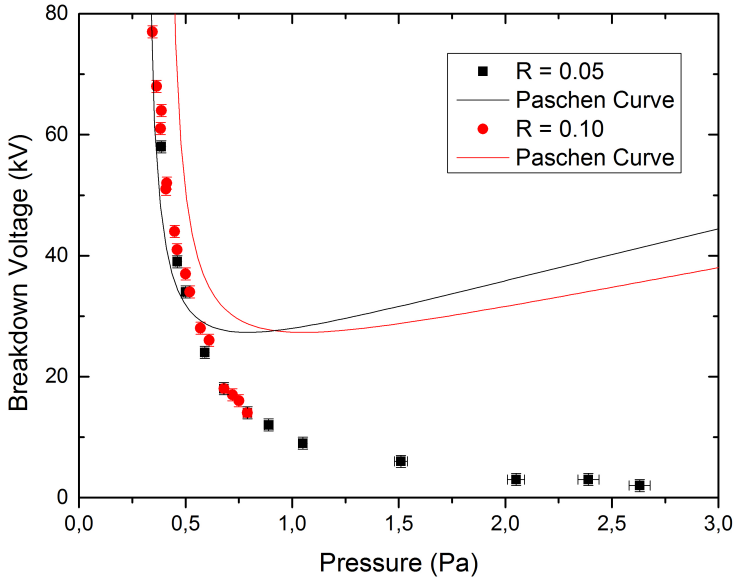

Figure 4.1: Breakdown voltage as a function of pressure

It is evident that a sperical geometry is not well modelled by Paschen's theory, the left asymptotes however seem to roughly coincide. Allthough not completely apparent from fig 4.1 the 0.10 m grid is able to operate in a slightly lower ($\pm 0.05\ Pa$) pressure regime. To compare the breakdown characteristics with the literature the breakdown voltage was plotted as a function of $A \cdot (pd)^{-2}$. According to literature [4] this should yield a straight line through the origin with a slope of 0.21 $kV \cdot Pa^2 \cdot m^2 \cdot amu^{-1}$ independent of the grid geometry, as mentioned in section 2.4.

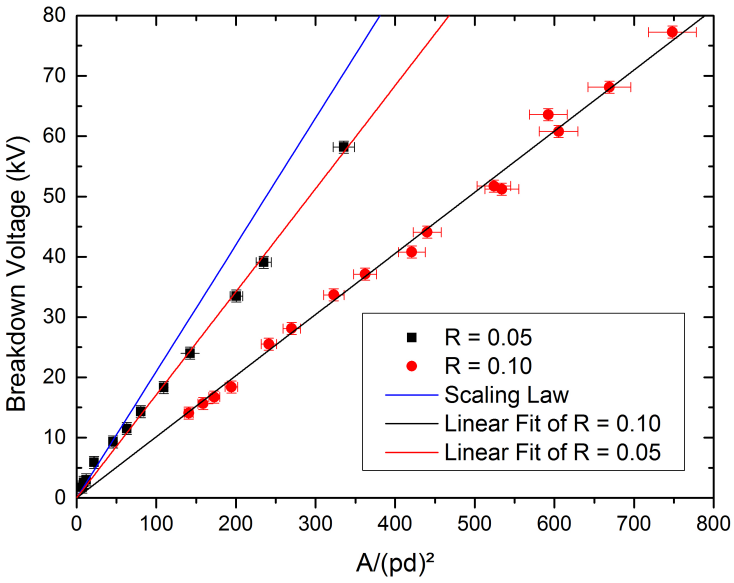

Figure 4.2: Scaling law plot of breakdown characteristics

Figure 4.2 shows the scaling law plot for both grids and the emperically derived scaling law from literature. The data points do indeed show a linear behaviour suggesting the breakdown voltage scales with $(pd)^2$. The slope of both linear fits are $(172 \pm 2) \cdot 10^{-3}$ and $(1013 \pm 8) \cdot 10^{-4}$ $kV \cdot Pa^2 \cdot m^2 \cdot amu^{-1}$ respectively.

4.2 Discussion

The breakdown characteristics for both grids are represented in figure 4.1 and 4.2. A striking result is the similar behaviour for both grids. Apparently the breakdown voltage is not a function of the radius nor the electrode distance, or both factors nullify each other's effect. The latter explanation however seems less likely, more as earlier research already suggested that the breakdown behaviour is at most a weak function of the grid radius [6]. As cited in [6] Miley and colleagues have shown that the breakdown behaviour is a function of the effective transparency. The similarity of the behaviour for both grids may imply that the effective transparency is also similar despite the fact that the geometric transparency differs by 5%.

Figure 4.2 shows a comparison of the breakdown data with the scaling law proposed by Hochberg [4]. It seems consistent with the p^{-2} behaviour however the slope of both fits are neither equal to themselves or to the scaling law. As was mentioned before the breakdown behaviour of both grids appears to be the same. Therefore a plot was made of the breakdown voltage as a function of the inverse of the pressure squared which can be seen in fig 4.3.

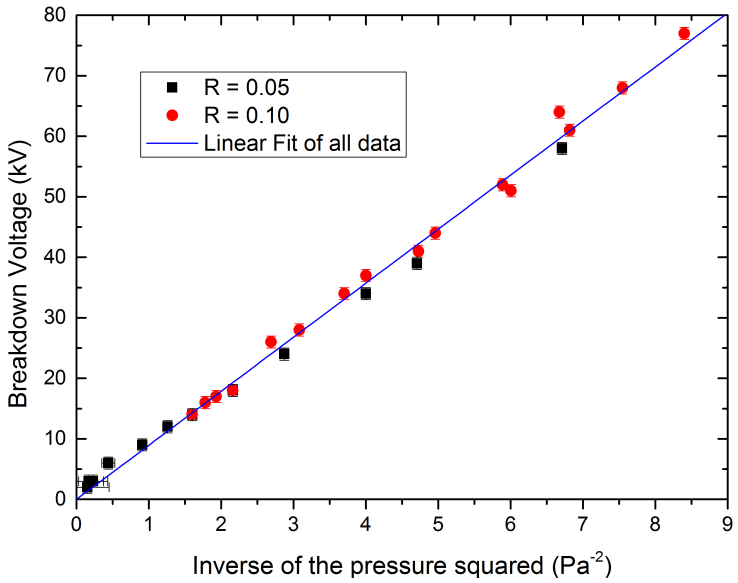

Figure 4.3: Breakdown voltage as a function of the inverse of the pressure squared

As all data points appear to lie on a straight line a linear fit was obtained of the combined data set resulting in a slope of $8.93 \pm 0.07\ V \cdot Pa^2$. This implies that the breakdown characteristics of the TU/e Fusor are indeed independent of both the cathode radius as well as well as the electrode separation. The latter in contrast to earlier research [4] [6]. An explanation for this can be found in figure 2.4, as the breakdown behaviour is dependent on the electric field. In a parallel plate geometry this is simply V/d as the potential profile is linear. In the spherical setup however the potential profile generally scales with r^{-1}. From figure 2.4 however it is apparent that the slope of the potential profile near the grid radius is similar for all three curves. Apparently the grid radius, nor the electrode distance affect the electric field near the cathode in this particular setup and therefore don't play a role in the breakdown behaviour.

5 Neutron Production Rate

This chapter will outline the results obtained from the measurements on the grids of $R = 0.05\ m$ and $R = 0.10\ m$. Unfortunately it was impossible to conduct any experiments with the grid of $R = 0.15\ m$ as a stable plasma in star-mode could not be obtained under any circumstance.

5.1 Results

Two types of measurements have been conducted to investigate the neutron production rate of the $0.10\ m$ and $0.05\ m$ grids. In the first measurement the NPR was measured as a function of the voltage in the $0.40 - 0.60\ Pa$ range at $0.05\ Pa$ intervals. Figure 5.1 shows the data for the $0.10\ m$ grid. Unfortunately it was impossible to conduct any experiments with the grid of $R = 0.15\ m$ as a stable plasma in star-mode could not be obtained under any circumstance. This chapter will outline the results obtained from the measurements on the grids of $R = 0.05\ m$ and $R = 0.10\ m$.

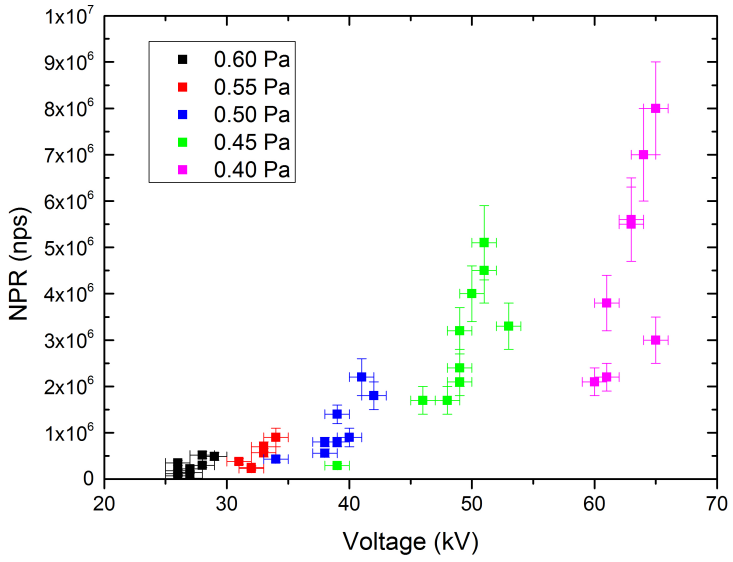

Figure 5.1: NPR as a function of voltage at different pressure for R = 0.10 m

Figure 5.1 shows that for every pressure the voltage range is confined to a small window yet there is quite a large spread in the NPR. While it is apparent that the fusion rate increases for lower pressures and higher voltage it is impossible to more clearly determine any straightforward relationship. Equation 2.13 showed that the fusion rate is linearly dependent on the current and the pressure). Dividing the fusion rate by both parameters and plotting against the voltage for both grids leads to an power law as can be seen in 5.2 below.

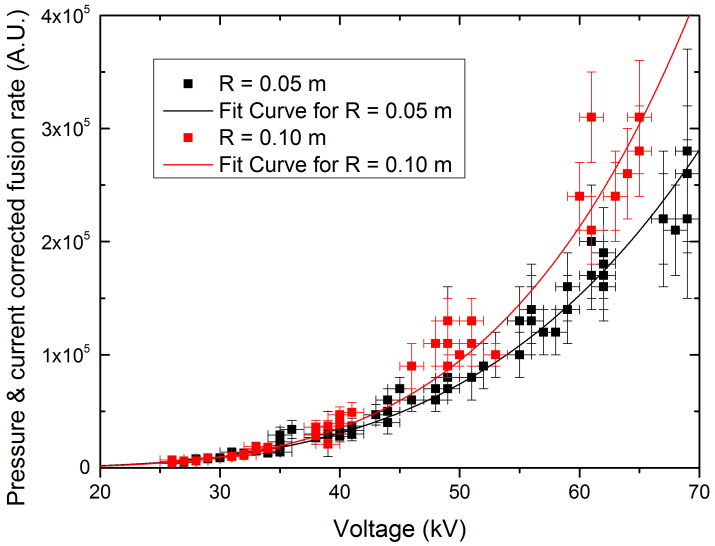

Figure 5.2: Pressure and current corrected NPR as a function of voltage for grid R = 0.10 m and R = 0.05 m

Both data sets were fitted with a power law curve ax^b, the data are given in the table below.

Grid Radius [m]	a	b
0.05	0.014 ± 0.003	3.96 ± 0.06
0.10	0.0027 ± 0.0009	4.44 ± 0.09

Table 5.1: Power law parameters for R = 0.05 m and R = 0.10

To further investigate the power law behaviour a separate loglog-plot was obtainend for both grids as can be seen in figures 5.3 and 5.4. From these figures it is apparent that both data sets show a linear behaviour in the loglog-plot. However for $R = 0.05\ m$ it tends to deviate at lower voltages. The slopes obtained from the linear fits are 3.90 ± 0.06 and 4.44 ± 0.09 nearly equal to the exponents obtained in the power law fit as was to be expected.

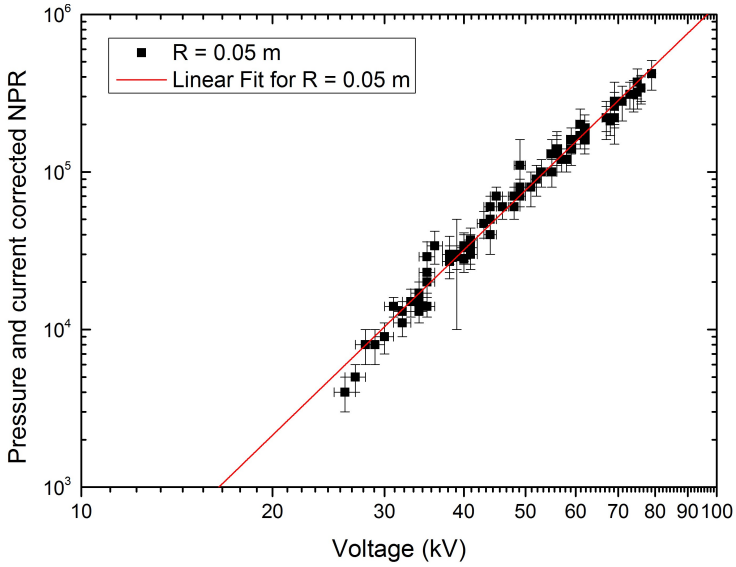

Figure 5.3: Loglog-plot of p and I corrected NPR vs. voltage for R = 0.05 m

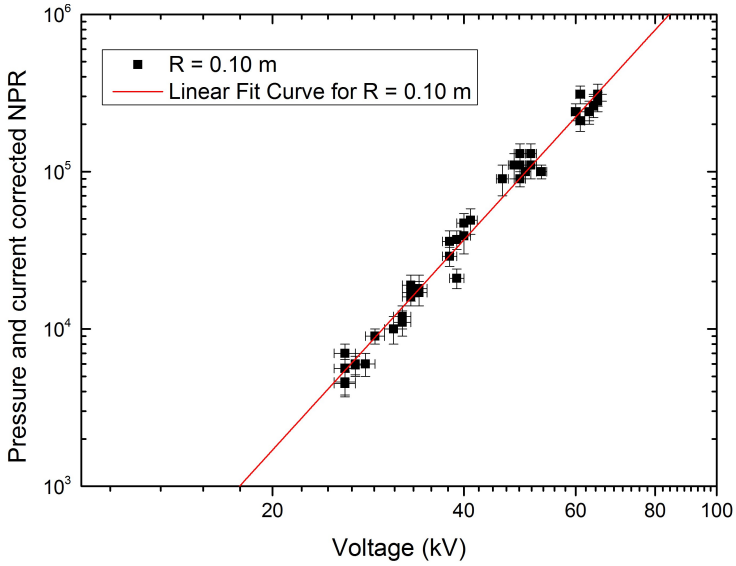

Figure 5.4: Loglog-plot of p and I corrected NPR vs. voltage for R = 0.10 m

For the second measurement the PSU voltage was kept constant (85 kV and 80 kV respectively) while the pressure was varied. Figure 5.5 shows the NPR as a function of the pressure for both grids. The NPR seems to increase with decreasing pressure up until a certain point. For $R = 0.05\ m$ the NPR decreases again for pressures below 0.42 Pa, for $R = 0.10\ m$ there are not enough data points although the flattening of the curve might imply a decrease for lower pressures as well.

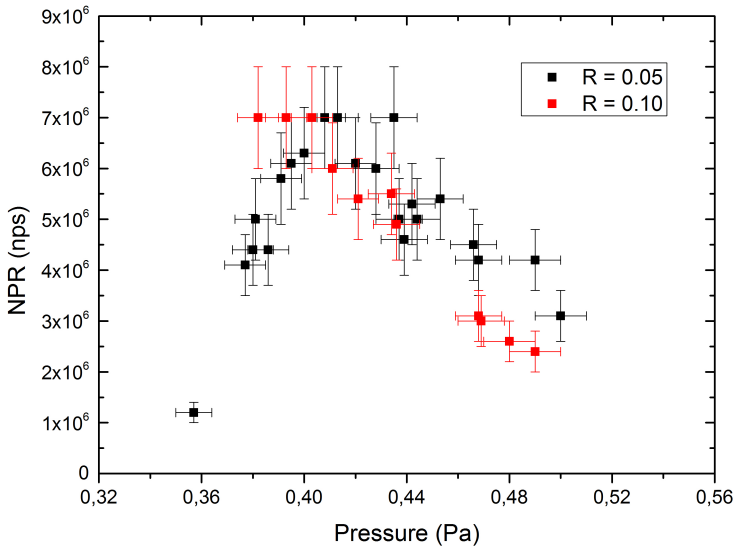

Figure 5.5: NPR as a function of pressure for R = 0.10 m and R = 0.05 m

As mentioned before the current and indirectly the Fusor voltage are dependent on the pressure, therefore a NPR versus voltage plot was also obtained.

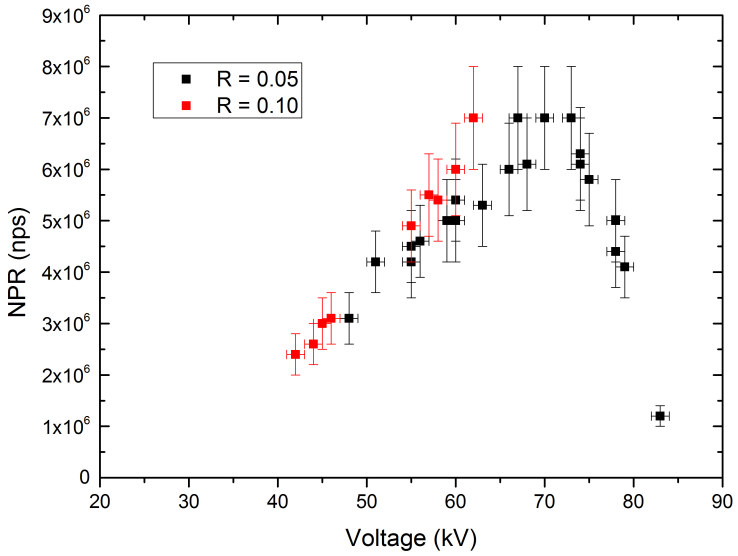

Figure 5.6: NPR as a function of voltage for grid R = 0.10 m and R = 0.05 m

Figure 5.6 shows the same relationship as figure 5.5 only mirrored as the voltage and pressure are inversely related. In the hopes of obtaining a more clear relationship again a correction was made for the pressure and the current resulting in figure 5.7. Both datasets were fitted with the power law, the fit data are given in table 5.2.

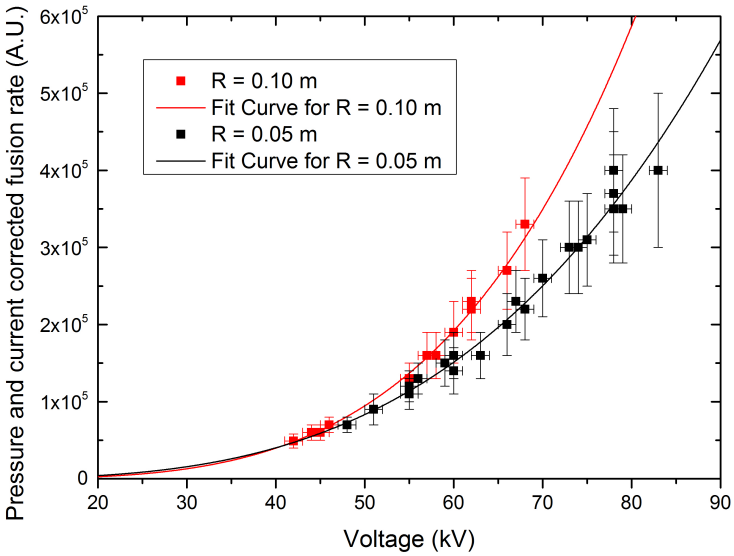

Figure 5.7: Pressure and current corrected NPR as a function of voltage for R = 0.10 m and R = 0.05 m

Grid Radius [m]	a	b
0.05	0.23 ± 0.08	3.27 ± 0.08
0.10	0.024 ± 0.008	3.88 ± 0.08

Table 5.2: Power law parameters for R = 0.05 m and R = 0.10

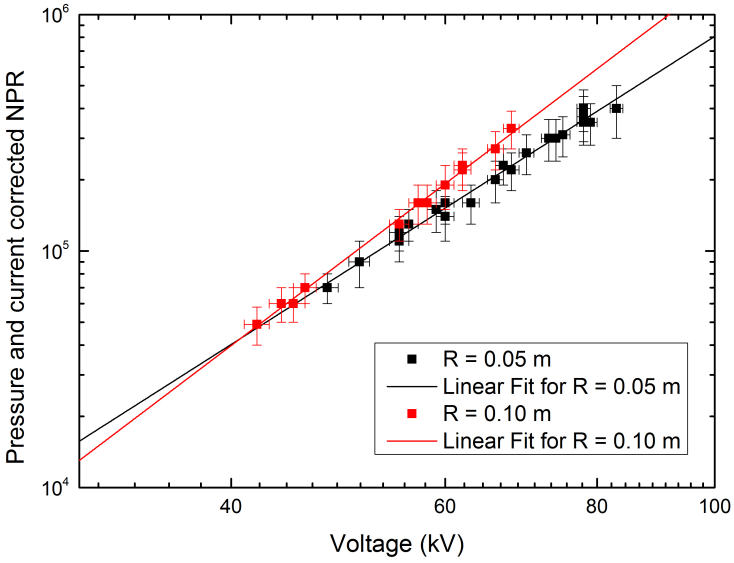

Figure 5.8: Loglog-plot of p and I corrected NPR vs. voltage for both grids

To investigate the power law behaviour again a loglog-plot was obtained for the pressure and current corrected NPR as a function of the voltage. The data sets for both grids show a clear linear behaviour in the loglog-plot. The slopes of the linear fits are 3.27 ± 0.08 and 3.88 ± 0.08 allmost exactely the exponents of the power law fit as is to be expected.

5.2 Discussion

The first neutron production measurement yielded data with a wide spread in NPR as is shown in figure 5.1. Equation 2.13 states that the fusion rate and therefore the neutron production rate is linear in both the pressure and the current in an attempt to reduce the spread the NPR was divided by both parameters. The same approach has been used in the second experiment. The reduced spread in figures 5.2 and 5.7 shows that this approach is successful.

Figures 5.2 and 5.7 both show a strong non-linear trend in the corrected NPR significantly favouring the larger grid. In both experiments the resulting data was fitted with a power law resulting in the parameters given in tables 5.1 and 5.2. Comparing the data in both tables two things are apparent. Firstly the grid with $R = 0.10\ m$ has indeed a larger exponent in both experiments. Furthermore the difference in the exponent between the two grids is 0.5 ± 0.2 for the first measurement and 0.6 ± 0.2 for the second. This might imply that the grid radius has an effect on the way the neutron production scales with V. It is also very well possible that the fusion rate scales with V^3 or V^4 and the coefficient a has to be adjusted. However as there is no theoretical consensus on how the fusion rate should scale with the voltage it is very difficult to numerically extract a more concrete relationship. Theoretically the factor $< \sigma v > / < v >$ accounts for the voltage scaling. In the parameter range of the experiments in this report the fusion cross-section is a linear function of the energy as can be seen in figure 5.9 below. As $E \sim v^2$ the factor can be reduced to $< v^3 > / < v >$. However little can be concluded without an analytical expression for the velocity distribution.Because of these unknown relationships it also not possible to asses the exact effect of the grid radius on the fusion rate.

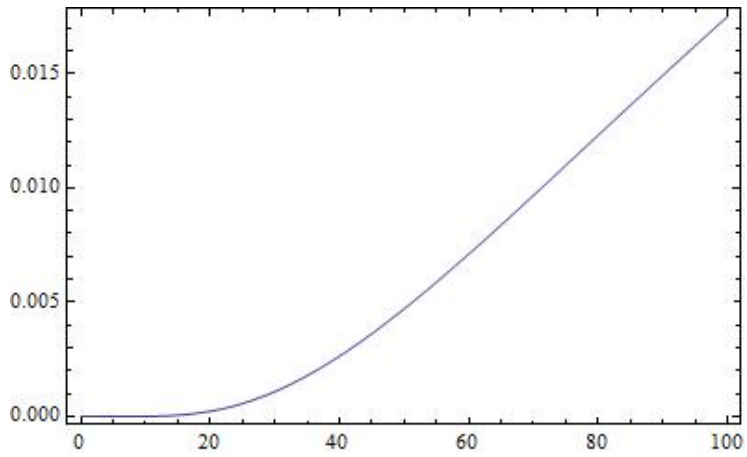

Figure 5.9: $\sigma(E)$ in Barns as a function of E in keV

6 Anomalies

Next to the regular results from the experiments some other observations of seemingly anomalous behaviour were documented. Some could possibly shed some light on the core data others are merely interesting, yet both are worth investigating more deeply.

One of the striking observations is the behaviour of the NPR in the second NPR experiment (where the pressure is varied at constant voltage). In figure 5.5 the NPR for $R = 0.05\ m$ increases with decreasing pressure, but decreases again below $0.41\ Pa$. As mentioned before the pressure, voltage and current are all interrelated in this set-up. Correction of the NPR for current and pressure have already shown that this changes the behaviour to a monotonous function. To further investigate the interdependence of the pressure, voltage and current the current and the voltage were plotted as a function of the pressure. For these plots data from the second NPR experiment was used.

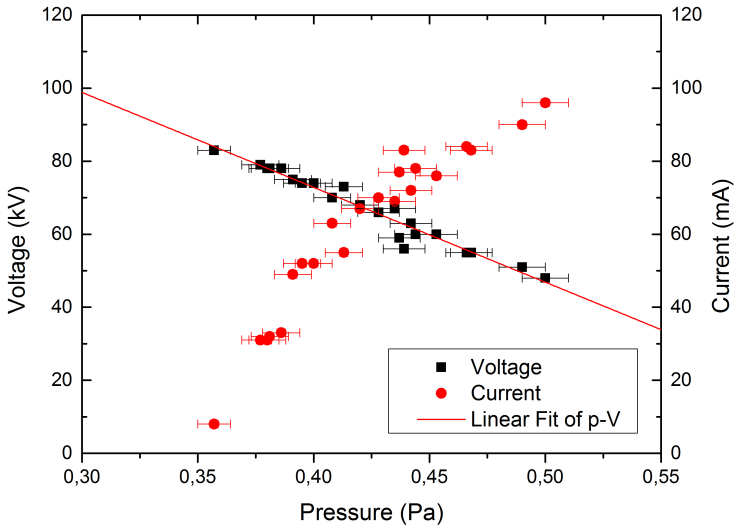

Figure 6.1: Voltage and current as a function of pressure for R = 0.05 m

Figure 6.1 shows that the current decreasingly increases with the pressure, while the voltage seems to decrease linearly. The voltage is only directly affected by the current and therefore indirectly by the pressure. The relationship between the fusor voltage and the current is caused by the resistance stack.

$$V_{Fus} = V_{PSU} - I \cdot R_r \tag{6.1}$$

Because of this linear relationship the voltage should decreasingly decrease with the pressure similar to the current. Figure 6.1 therefore suggests that for some reason the voltage has decreased more than expected. Figure 6.2 shows the voltage as a function of current for $R = 0.05\ m$, the red line is a representation of equation 6.1 with $V_{PSU} = 85\ kV$ and $R_r = 0.21 \cdot 10^6\ \Omega$. Below 50 mA the data points follow equation 6.1, however as current further increases the voltage drops markedly. This suggests that the PSU is unable to sustain these high voltages while simultaneously supplying a high current. While this behaviour is expected near the current limit of 100 mA, its occurrence around 50 mA suggests a defect in the power supply.

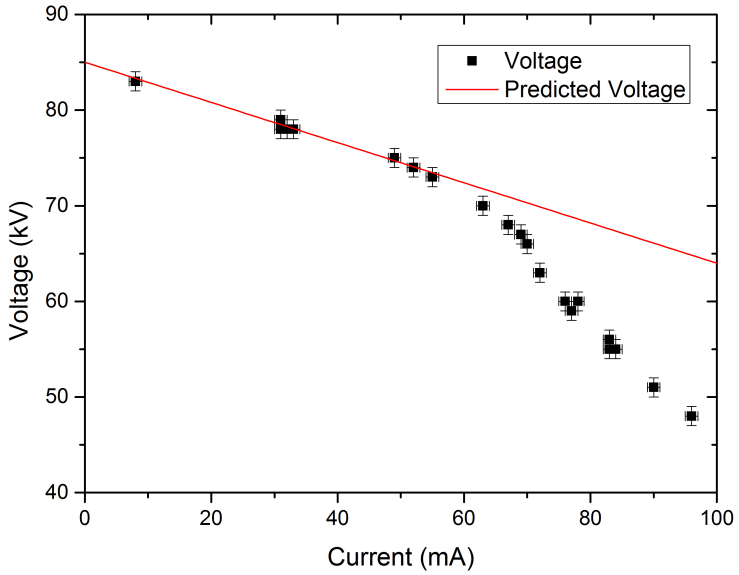

Figure 6.2: Voltage as a function of current for R = 0.05 m

A last remarkable observation concerns the behaviour of the pressure during operation. The attentive reader might have already noticed the apparent drop in pressure as can be see in figures 3.2 and 3.3 which normalizes as soon as operation is terminated. As the pressure gauge is positioned at the edge of the vacuum vessel one of the proposed explanations is that the general inward motion of the ions creates a pressure gradient in radial direction which results in a relatively lower pressure at the edge of the vessel. Figure 3.2 shows an a quick oscillation of the pressure signal which is assumed to be an artefact. One explanation is the radiation levels near the fusor which could interfere with the electronics. Figure 3.3 furthermore shows sudden changes in pressure for which there is no explanation as of yet.

7 Conclusion

The preview chapters included an overview of the theory, the results and a discussion of the results. This chapter will summarize the findings shed some light on the implications and put forth some suggestions for further research and improvement on the TU/e Fusor.

7.1 Summary

The goal of this report is to investigate the effect of the cathode radius on the neutron production. Based on theoretical calculations it was expected that the fusion rate and therefore also the NPR would scale linearly with the cathode radius. Several experiments have been conducted with different cathode radii. Comparison of the data indeed showed that increasing the grid size increases the NPR. However as only two grids could be compared it still remains unclear if this increase is a monotonous function of the cathode radius or if it reaches a maximum at a certain radius. The latter can reasonably be expected based on the current knowledge of IEC devices. It was also impossible to obtain a quantitative measure of this effect as there is insufficient information about the relationship of between the fusion rate and the voltage, which is expected to be connected to the velocity profile. The data now points to an exponential or power law behaviour in the voltage, with the NPR scaling roughly with the voltage to the 3^{rd} to 4^{th} order. The data used in this report are still ambiguous about the exact scaling. Either the exponent is a fixed value and the grid radius has a linear or otherwise non-exponential effect or the grid radius somehow has an effect on the exponent. More research is needed on this subject.

There is also very little known about the confinement, transparency and recirculation. In this text the geometric transparency was used to calculated the recirculation as a measure of the confinement. However, research has shown that microchannels play an important role, resulting in an effective transparency, for which there is no quantitative measure as of yet.

Preliminary measurements regarding the breakdown characteristics have established that the breakdown voltage is a function of the inverse of the pressure squared. This is in part in agreement with the literature. The data in this report however show that the breakdown voltage is neither a function of the cathode radius nor the electrode distance d the latter which does play a roll in Hochberg's scaling law [4]. The particular vacuum potential profiles (fig. 2.4) for the TU/e Fusor might explain the absence of d in the breakdown behaviour as the electric field near the cathode is similar for different grid radii.

7.2 Recommendations

As is often the case in research this work raises more questions than answers. It has shown that increasing the grids radius leads to an increase in the fusion rate. However more research is needed on several aspects of IEC fusion devices for a more conclusive interpretation of the data. One of the missing elements that is key to predicting the fusion rate is the velocity profile of the ions in the plasma. As the velocity profile is at least in part a function of the voltage this may shed some light on the relationship of the fusion rate and the voltage and indirectly help quantify the influence of the cathode radius.

Another important but still ill-understood factor is the confinement and more specifically the effective transparency and the resulting recirculation. More research is needed on the formation of microchannels, their effect on the transparency as well as a means to measure this transparency.

Lastly the anomalous drop in the pressure signal needs further investigation. If it is in fact caused by a pressure gradient sustained by the nett inward motion of the ions it might prove to be a way for measuring the ionisation.

Apart from future research there is also room for improvement on the TU/e Fusor setup. One of the main practical problems encountered during the experimental work is the interdependence of all three main parameters. The voltage and current are both dependent on each other and the current is also dependent on the pressure. This makes it difficult to perform experiments with properly controlled parameters. One solution to this problem is to decouple the voltage and current (at least in part) by switching to ion injection as the main ion source. Another advantage of ion injection is the ability to operate at significantly lower pressures greatly reducing loss reactions. Although the beam-background fusion will be similarly reduced it is believed that bea- beam fusion dominates at lower pressures and could potentially outperform current (beam-background) fusion rates. [9] Another area of improvement is the PSU. As already mentioned in the discussion it appears that the PSU is unable to supply high currents at high voltages. Whether this is actually the case and what causes it needs to be further investigated. Considering the non-linear scaling of the NPR with the voltage improving the power supply may be beneficial in its own right.

Bibliography

[1] ML Oliphant. Tranmutation effects observed with heavy hydrogen. (133):413, 1934.

[2] TH Rider. A general critique of inertial-electrostatic confinement fusion. 2, 1995.

[3] ECG Hermans. Design and optimization of an inertial electrostatic confinement fusion device, 2013.

[4] TA Hochberg. Characterization and modeling of the gas discharge in a sfid neutron generator, 1992.

[5] A Von Engel. *Ionized Gases*. Oxford University Press, 1955.

[6] George H. Miley and S. Krupakar Murali. *Inertial Electrostatic Confinement (IEC) Fusion*. Springer, 2014.

[7] BJ Egle, JF Santarius, and GL Kulcinski. Comparison of spherical and cylindrical cathode geometries in inertial electrostatic confinement devices, 2006.

[8] AL Wehmeyer, RF Radel, and GL Kulcinski. Optimizing neutron production rates from d-d fusion in an inertial electrostatic confinement device, 2004.

[9] Thomas J. McGuire. Improved lifetimes and synchronization behavior in multi-grid inertial electrostatic confinement fusion devices, 2007.